Water around fullerene shape amphiphiles: A molecular dynamics simulation study of hydrophobic hydration

S. R. Varanasi, O. A. Guskova, A. John, and J.-U. Sommer

Citation: The Journal of Chemical Physics **142**, 224308 (2015); doi: 10.1063/1.4922322
View online: http://dx.doi.org/10.1063/1.4922322
View Table of Contents: http://scitation.aip.org/content/aip/journal/jcp/142/22?ver=pdfcov
Published by the AIP Publishing

Water around fullerene shape amphiphiles: A molecular dynamics simulation study of hydrophobic hydration

S. R. Varanasi,[1,a),b)] O. A. Guskova,[1,2,a)] A. John,[1] and J.-U. Sommer[1,2,3]
[1]*Institut Theorie der Polymere, Leibniz-Institut für Polymerforschung Dresden e.V., Hohe Straße 6, Dresden D-01069, Germany*
[2]*Dresden Center for Computational Materials Science (DCMS), Technische Universität Dresden, Dresden D-01069, Germany*
[3]*Institut für Theoretische Physik, Technische Universität Dresden, Zellescher Weg 17, Dresden D-01069, Germany*

(Received 4 May 2015; accepted 29 May 2015; published online 11 June 2015)

Fullerene C_{60} sub-colloidal particle with diameter ~1 nm represents a boundary case between small and large hydrophobic solutes on the length scale of hydrophobic hydration. In the present paper, a molecular dynamics simulation is performed to investigate this complex phenomenon for bare C_{60} fullerene and its amphiphilic/charged derivatives, so called shape amphiphiles. Since most of the unique properties of water originate from the pattern of hydrogen bond network and its dynamics, spatial, and orientational aspects of water in solvation shells around the solute surface having hydrophilic and hydrophobic regions are analyzed. Dynamical properties such as translational-rotational mobility, reorientational correlation and occupation time correlation functions of water molecules, and diffusion coefficients are also calculated. Slower dynamics of solvent molecules—water retardation—in the vicinity of the solutes is observed. Both the topological properties of hydrogen bond pattern and the "dangling"–OH groups that represent surface defects in water network are monitored. The fraction of such defect structures is increased near the hydrophobic cap of fullerenes. Some "dry" regions of C_{60} are observed which can be considered as signatures of surface dewetting. In an effort to provide molecular level insight into the thermodynamics of hydration, the free energy of solvation is determined for a family of fullerene particles using thermodynamic integration technique. © *2015 AIP Publishing LLC.* [http://dx.doi.org/10.1063/1.4922322]

I. INTRODUCTION

The study of molecular and aggregate properties of fullerenes in a liquid environment is a problem deserving increasing theoretical interest. The C_{60}-solvent interactions and fullerene solubility are a primary factor contributing to the rapid advancement of fullerene chemistry for material science applications.[1,2] First of all, the extraction and purification of fullerenes from impurities require the sensible choice of solvents for the chromatographic separation. Second, fullerenes that combine unique geometrical and electronic properties are extremely promising components for use in solution-processable organic thin-film transistors and bulk heterojunction solar cells. Depending on the nature of solvents and solvent composition, concentration of solution, solvent annealing conditions, etc., a thin film morphology, i.e., supra-molecular structure of phase-separated systems with specific grain size and shape, molecular ordering in pure phases, film roughness, and porosity, can be drastically changed, and hence, the device performance can be improved.[3–5] Moreover, fullerenes in dissolved state and as colloidal suspensions can be exploited in various medical fields.[6,7] Specifically, the solubility, aggregation, and solvation of fullerenes are directly related to their functions in biosystems.[8–20]

In a liquid environment—polar or non-polar—the control over the generation of fullerene clusters is a challenging multiscale problem that simultaneously involves a hierarchy of processes on very broad time and length scales.[21–28] Thus, in-depth knowledge of the origin, magnitude, and sign of solvent-mediated interaction from the molecular standpoint is of vital importance for the investigation of aggregation processes which begin on a single molecular level with the formation of a contact fullerene pair. On the other hand, solute-solvent interactions may also play an important role both in direct dispersion of fullerenes from the solid sample in water and in stabilization of resulting colloidal systems.[25]

The solvation of a single non-polar substance in aqueous media remains a controversial issue if judged by the number of different theoretical approaches proposed so far. The classical mechanism for hydrophobicity predicts the water structuring near nonpolar solute ("iceberg" model).[29,30] According to an alternative theoretical description ("void volume" model),[31–33] small hydrophobic solutes (less than 1 nm in diameter, molecules of inert gases, methane, etc., similar in size to the substances studied by Frank and Evans) are accommodated in water hydrogen network with minor perturbations to water structure, and their hydration is captured accurately by density fluctuations of pure water (caging hydration, static ice-like "clathrate" structure). In contrast, water around a large

[a)]Authors to whom correspondence should be addressed. Electronic addresses: s.raovaranasi@uq.edu.au and guskova@ipfdd.de
[b)]Present address: School of Chemical Engineering, University of Queensland, St Lucia QLD 4072, Australia.

hydrophobe (>1 nm in diameter) fails to form the persistent hydrogen bonds network and solute hydration is accompanied by dewetting their surfaces (drying, the formation of vapor-like layer in contact with the solid surface of a hydrophobe). The conclusion about length-scale dependence of hydrophobic hydration has affected modern models of hydrophobic effect, such as inhomogeneous solvation theory describing thermodynamics of water around chemically heterogeneous solute surface/cavitity.[34]

The hydration of fullerene C_{60} sub-colloidal particle with diameter ~1 nm is even more intriguing because this carbon structure represents a boundary case between small and large hydrophobic solutes on the length scale of "water-fearing" hydration,[35–38] and for this particular system, the question "caging vs. drying" remains unsettled. Moreover, fullerene demonstrates the "non-conventional" hydrophobic character: on the one side, fullerenes are insoluble in water suggesting their hydrophobicity on macroscale; on the other side, their pair-wise effective interaction in aqueous solution includes a repulsive solvent-induced contribution, as it follows from the calculation of the potential of mean force by several independent research groups.[36,38–41]

A comprehensive research on the factors of fullerene solvation or self-organization in solution requires a complete set of physico-chemical properties, including solubility, solvation free energy, and entropy changes for a more realistic description of the solvated system. Although most of these data can be obtained experimentally,[26,42–45] this approach is still hampered by extremely low solubility of fullerenes in water (7.96 ng/l) and a high level of aggregation. Therefore, most previous experiments concerning factors of solvation focused on colloid rather than molecular C_{60}-form (a true solution). Thus, a viable alternative to the real experiment is the computational one.

In the present article, we discuss the results of full-atomistic molecular dynamics simulation of fullerene and its amphiphilic-C_{60} derivatives in water. The investigated systems are pristine C_{60}, phenyl-C_{61}-butyric acid methyl ester (PCBM; properties of an isolated molecule,[46,47] solid state organization as pure crystals and co-crystals,[48–55] and in liquid media[56,57]) and a homologues series of N-substituted fulleropyrrolidines (FPs), which differ in a number of straight methylene groups–CH_2– in a side chain. These molecules vary from each other in shape and polarity; therefore, they appear to be good candidates for the study of effects of functionalization on the hydration of fullerenes. Such hybrids based on various nanobuilding blocks with distinct geometries, chemical nature, and functions usually refer to "shape amphiphiles," because they behave in a similar vein to what is known for typical amphiphiles. The range of similarities and differences between the mentioned amphiphiles is well supported by numerous reports.[58,59]

This paper is organized as following. Section II describes the simulation setup used to imitate the carbon particles immersed in aqueous medium. In Sec. III, the DFT-calculations are described at first, followed by results from classical simulations. These include static and dynamical properties of water in the solvation shells of the solute, comparative study of free energy of solvation of fullerene derivatives, the description of translational diffusivity of particles, as well as peculiar properties of interfacial hydrogen bond network near carbon spheroid, and changes in the degree of hydration. The final part summarizes the results as well as discusses the general issues, which pertain to hydration properties of the fullerene-based molecules.

II. SIMULATION SETUP AND COMPUTED PROPERTIES

One of the principal ideas in chemistry is that "the shape" of the molecule (both the geometry and electron distribution) is central to function.[60] The fullerene derivatives have a rigid spheroid core and well defined geometrical characteristics, whose impact on the final architecture of the nanostructures has been described recently.[61] Here, we extend our previous work[57] and provide a description of the second component in molecular "shape" of fullerenes—molecular electrostatic potential (MEP). The MEP as an indicator of the charge distribution in a molecule is a useful tool that has been employed to understand a variety of chemical and physical phenomena in fullerene material science, in particular, solvent effects[62] and supramolecular structures.[63,64]

The geometry of fullerenes—phenyl-C_{61}-butyric acid methyl ester and fulleropyrrolidine cations—in vacuum at 0 K is obtained from density functional theory with B3LYP/6-31G(d,p) basis set in Gaussian 09 software.[65] Cartesian coordinate gradients are optimized to less than 10^{-6} a.u. as convergence criterion. Vibrational frequencies are evaluated by numerical differences of analytical gradients. None of predicted vibrational spectra have any imaginary frequency, which proves that optimized geometry is located at the local minimum on the potential energy surface. The corresponding geometries of individual components are shown in Fig. 1.

Molecular electrostatic potential surfaces (MEPSs, a plot of electrostatic potential mapped onto the constant electron density surface) are generated with B3LYP hybrid functional scheme using 6-31G(d,p) basis set in vacuum. Since it has been stated that MEP calculations are relatively insensible to the basis set,[66] we have not employed different basis sets. MEP-scalar $V(\mathbf{r})$ at a given point $\mathbf{r}(x, y, z)$ classically is defined as interaction energy between the electrical charge generated from the molecule electrons and a positive point charge as a

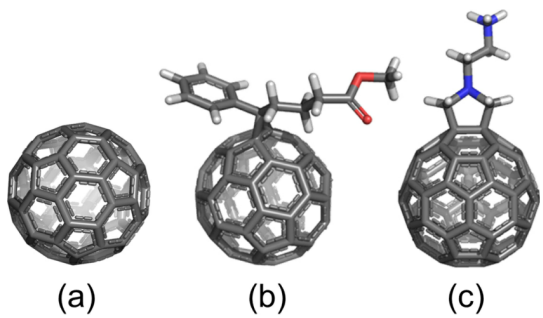

FIG. 1. Structures of pristine fullerene (a) and fullerene derivatives: (b) PCBM, (c) FP2 cation. Grey, red, white, and blue sticks represent carbon, oxygen, hydrogen, and nitrogen atoms, respectively. For fulleropyrrolidine, the "attached" organic moiety is 2-pyrrolidin-1-ylethylammonium. Chloride anion of FP2 is omitted.

probe located at **r**, supposing that the molecule is not polarized by the test charge,[67]

$$V(\mathbf{r}) = \sum_{A=1}^{N} \frac{Z_A}{|\mathbf{R}_A - \mathbf{r}|} - \int \frac{\rho(\mathbf{r}')\mathrm{d}^3 r'}{|\mathbf{r}' - \mathbf{r}|}, \quad (1)$$

where Z_A is the charge of the nucleus A, which is considered to be a point charge located at $\mathbf{R}_A$, the second term $\rho(\mathbf{r}')$ is the electron density function, and r' is a dummy integration variable. The numbers indicate the interaction energy in a.u. between positive probes on the molecule at that particular point. These values could be correlated to the electrostatic charges on the atoms with the negative number corresponding to negative charge and positive number corresponding to positive charge. MESP minimum (V_{min}) corresponds to a point at which electrostatic potential due to electron density term dominates maximally over the bare nuclear term and the value at the minimum quantifies the electron-rich character of that region, and vice versa for the MESP maximum (V_{max}). The MEPSs of the computed MEPs are generated using GaussView 5 program.[68]

In our MD simulations, we employed the PCFF (Polymer Consistent Force Field)[69] supplemented by some additional parameters related to fullerene nanoparticle. The total potential energy of the system is represented as a sum of the bonded terms (the energy contributions for bond, angle, torsion, out-of-plane angle coordinates, as well as the energy contributions for cross-coupling terms between internal coordinates) and non-bonded terms, which include a Lennard-Jones (LJ) potential for the van der Waals interactions and electrostatic (Coulombic) term.

For C_{60} cage, the constants for LJ potential are taken from the original parameterization of Girifalco ($\varepsilon = 0.2763$ kJ/mol, $\sigma = 3.469$ Å) reproducing the experimental crystal data of fullerenes.[70] This force field has proved its reliability for the investigation of structure and dynamics of C_{60} in aqueous, organic, and inorganic media.[39,40,56,71–75] Carbon atoms of C_{60}-cage are modelled as uncharged spherical particles with LJ interactions. For terminal ammonium group of the fulleropyrrolidine, the LJ parameters are borrowed from the OPLS-AA (Optimized Potentials for Liquid Simulations - All-Atom) force field.[76] A cutoff distance of 1.8 nm is employed for LJ interactions. The cross interactions between oxygen of water and fullerene atoms are also represented by LJ interactions with the energy and size parameters obtained from the individual parameters using the Lorentz-Berthelot mixing rules.[77] The electrostatic interactions are treated using particle mesh Ewald summation technique with a Fourier grid spacing of 0.3 nm, sixth-order interpolation, and a real-space cutoff of 1.8 nm. All electrostatic charges are kept fixed during the MD simulations.

The water molecules are modelled with modified three-site non-polarizable TIP3P model,[78] and O–H bonds ($k_b = 1882.8$ kJ/mol, $b_0 = 0.9572$ Å) and H–O–H angles ($k_\theta = 230.12$ kJ/mol, $\theta_0 = 104.52°$) are treated with harmonic potentials. This model has been successfully used in recent MD simulations of hydrating properties of pristine fullerenes/fullerene derivatives in aqueous medium or in binary water-containing solvents[36,79–87] and in simulations of C_{60}-complexes with biomacromolecules.[10,64,88,89]

To obtain a start configuration, bare fullerene or amphiphilic molecule (and counterion if needed) in optimized geometry is placed in a cubic box and then solvated with $n = 1000$ or 3000 water molecules, which are uniformly and randomly distributed over the simulation box. This number of water molecules is sufficient to solvate one fullerene molecule for further analysis.[38,90–93] To avoid any hydrogen bond contacts between solute and water molecules, the initial cubic simulation box is at least eight times larger than the volume corresponding to liquid water density 1 g/cm^3 (for n water molecules) at $T = 300$ K. As a reference system, we also calculate the TIP3P pure water confined in the same periodic box.

All start configurations are generated using PACKMOL software.[94] Unlike previous full-atomistic studies of hydration behaviour of fullerene or its derivatives, in which a single solute molecule has been placed at the center of a box and was rigid[95,96] and kept fixed/frozen during the simulation time,[73,74,97,98] the current research employs a model without any external constraints for carbon nanoparticles, because our primary goal as outlined above is to investigate not only the spatial distribution and dynamics of water around a hydrophobe but also to characterize both the diffusion of nanoparticle and the micellization processes. The latter aspect is described in details in our recent publication.[57]

All MD simulations are performed using LAMMPS software.[99] At the beginning, all MD runs are carried out in NPT ensemble: equilibration time for 500 ps (integration step 0.01 fs, $T = 300$ K, stochastic velocity rescaling thermostat for temperature control) and production run for at least 2.5 ns (integration step 1 fs, $T = 300$ K, Nosé-Hoover thermostat for temperature control) or until the volume of the system reaches an equilibrium value to obtain the correct density (pressure $P = 1$ atm). The equilibration is tested by monitoring thermodynamic properties like temperature, pressure, and energy oscillations. The equilibration time is in each case much larger than the structural relaxation time τ for pure TIP3P water at temperature T. Starting from this configuration, the simulations are performed in NVE ensemble for 1 ns after an equilibration run of 1 ns (integration step 1 fs). Further, statistical data are collected every 0.01 ps for duration of 3 ns, which leads to fairly convergent results for all subsequent analyses described in Sec. III.

In order to explore the spatial arrangement of water molecules around the solute surface, the radial distribution functions (RDFs) in one dimension for the center-of-masses of region of interest (C_{60} spheroid, side chains, counterion, etc.) to water O atom and water H atom are calculated.[77] Among all possibilities, the RDFs between center-of-masses are used to define both the solvation shells around different regions of solute and coordination numbers. In the case of a liquid system, this coordination is the average number of molecules in any given solvation shell. Hence, by a spherical integration of each peak, the average number of water molecules n in each layer can be evaluated,

$$n(r) = 4\pi\rho \int_0^r r'^2 g(r')\,\mathrm{d}r'. \quad (2)$$

Here ρ is the bulk number density, r' is the distance between the two species under consideration, and r is the distance

corresponding to the first minimum in the RDF between the given species (the first solvation shell).

The orientation of water molecules near a hydrophobic fullerene surface/region of interest in the first solvation shell is described by distributions of two angles θ and ω, and the definitions of which are given in Fig. 2.[100]

The change in Gibbs free energy of solvation ΔG_{solv}, the energy to transfer a solute from its vapor phase (vacuum) to a solvent, is calculated from MD simulations using thermodynamic integration (TI) technique[101] implemented in Material Studio 7.0 (COMPASS force field,[102] NPT ensemble, $P = 1$ atm, $T = 298$ K). In this method, the interaction of the molecule with solvent is gradually increased from zero to full interaction in a number of steps, i.e., the fullerene is gradually "grown" into the solvent. For each coupling strength λ, a simulation is performed and the derivative of the solvation free energy is calculated, and then the free energy is obtained as the integral,

$$\Delta G_{solv} = \int_{\lambda=0}^{\lambda=1} \left\langle \frac{\mathrm{d}H(\lambda)}{\mathrm{d}\lambda} \right\rangle \mathrm{d}\lambda, \tag{3}$$

where H is the parameterized Hamiltonian.

The calculation of Gibbs free energy of solvation ΔG_{solv} is carried out over three runs[103] using Eq. (3). The first one ΔG_1 is the calculation of the "ideal" contribution—starting from a solute molecule in vacuum, the charges are gradually reduced to zero, whilst keeping all other interactions the same. The second one ΔG_2, called van der Waals term, is calculated when the "chargeless" solute molecule is coupled to the solvent by switching on the van der Waals interactions in a number of steps, i.e., the free energy required to place an uncharged van der Waals cavity into solution. Finally, the charges are re-introduced on the solute molecule immersed in solvent. The free energy ΔG_3 of this step is the electrostatic contribution, i.e., the free energy of charging the cavity once it has been placed into solution. The total ΔG_{solv} energy is the sum of ideal, van der Waals, and electrostatic terms. For each thermodynamic state, 20 simulations are performed, varying the value of the coupling parameter λ. For each λ value, the simulation runs of 1 ns are performed. All the start configurations are taken from MD simulations described above. The free energy to transfer fullerene from its vapor phase (vacuum) to octane is calculated for comparison. The number of octane molecules in a cubic simulation cell is 800 (density 0.703 g/cm^3). The $\Delta\Delta G^t$ energy to transfer fullerene molecule from organic to aqueous phase is defined as well.

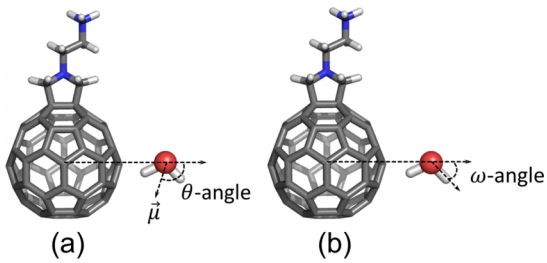

FIG. 2. Schematic representations of angles defined to study the orientation of water molecules near a hydrophobe (fulleropyrrolidine as an example): (a) θ, the angle between vector joining center-of-masses (of region of interest, here—fullerene cage)—oxygen of water molecule and dipole moment vector of water molecule $\vec{\mu}$ and (b) ω, the angle between vector joining center-of-masses (of region of interest, here—fullerene cage)—oxygen of water molecule and O–H-vector of water molecule. For the color scheme, see Fig. 1.

To define the translational and reorientational dynamics of the solvent molecules in the vicinity of nanoparticle surface, several time correlation functions are computed,

$$C^{\alpha}(t) = \frac{\sum_{i=1}^{N} [\vec{\alpha}_i(t+t_0) \cdot \vec{\alpha}_i(t_0)]}{\sum_{i=1}^{N} |\vec{\alpha}_i(t_0)|^2}, \tag{4}$$

where $\vec{\alpha}_i$ is a vector of interest (velocity $C^{vv}(t)$, dipole moment $C^{\mu}(t)$, OH vector $C^{\mathrm{OH}}(t)$, etc.). Function (4) is calculated only if the solute molecule stays in the region of interest for at least 2 ps otherwise it is not considered for the calculation, in contrast to the methodology used in the previous studies.[97] This procedure is applied to avoid re-crossing events from one region to another, for example, from solvation shells to bulk water and vice versa. The velocity autocorrelation functions (VACFs) are calculated up to a time interval of 2 ps and the reorientational correlation functions—up to 25 ps only for those water molecules which satisfy the above mentioned criterion. These reorientational correlation functions exhibit stretched exponential decay, as discussed in Sec. III. The latter also known as Kohlrausch-Williams-Watts (KWW) law is widely employed in the characterization of the non-exponential nature of relaxations in several phenomena in complex condensed matter systems,[104,105] and recently, it has been used to explain the residence times of the hydration water of proteins, confined water near inorganic surfaces and pores, and fullerene-containing systems.[74,97,106,107] The KWW function is given by[108,109]

$$C_{\beta}(t) = Ae^{-(t/\tau)^{\beta}}, \tag{5}$$

where A, β, and τ are prefactor, stretched exponential constant, and central relaxation time, respectively. The KWW time constant τ provides the time scale over which the process involves: in our case, it gives an estimate of the residence time of waters in the considered solvent layer. The stretched exponential constant β varies between 0 and 1. The average relaxation time $\langle\tau\rangle$ is evaluated by using the following equation:

$$\langle\tau\rangle = \frac{A\tau}{\beta}\Gamma\left(\frac{1}{\beta}\right), \tag{6}$$

where Γ denotes Gamma function.

The diffusion coefficients D of solvent molecules both in pure water and in hydration layer around the solute are calculated from velocity autocorrelation functions using Green-Kubo relations.[110] The diffusion constants for fullerenes D_f in solutions are obtained from the mean square displacement in the linear time regime by the Einstein relation,

$$D_f = \frac{1}{6t}\langle r\rangle^2, \tag{7}$$

where $\langle r\rangle^2$ is the mean square displacement of the center-of-mass of fullerene spheroid in water. The linear fit ranges from 35 to 500 ps.

To describe hydrogen bonding, the definition suggested by Luzar and Chandler is applied, which identifies H-bonds as having an O · · · O distance less than 3.5 Å and an OH · · · O angle less than 30°.[111] Image rendering and visual inspection are performed with VMD,[112] PyMOL,[113] and DS Visualizer.[114]

III. RESULTS AND DISCUSSION

A. Results of DFT calculations

The atomic configurations of C_{60}, PCBM, and FP2 after geometry optimization are presented in Fig. 1. The bond lengths, angles, and dihedrals of fullerene and PCBM molecules coincide with QM results described in Refs. 46 and 47. The geometry and HOMO/LUMO pattern of a common structural fragment of FP2 are in agreement with predictions by Zhang and co-workers.[115]

Substitution of a fullerene spheroid with a side chain is expected to change not only the symmetry of this molecule but also the charge distribution. This can be better understood by creating MEPS plots because they allow 3D visualization of different charge distributions of molecules and are particularly useful for understanding the hydration process (Fig. 3). Specific values of electrostatic potentials at the surface are represented by different colors in accordance to the scale. The blue color represents an area of low electron density and has a positive charge. On the other hand, area of red color is characterized by an abundance of electrons and has negative charge. An important feature evident from Fig. 3 is that the functionalization of carbon spheroid with positively charged group not only changes electron density at the attachment site but also spreads over several adjacent carbon atoms, affecting their charges. This inductive effect vanishes with lengthening side chains (Fig. S1[103]): starting from FP2 (c) (Fig. S1[103]), the terminal $-NH_3^+$ group affects mainly atoms of the addend, and its influence on the fullerene spheroid becomes lower and disappears.

The Mulliken charges on adjacent to the addend carbon atoms are illustrated in Fig. 4. The atomic charges i vary from −0.097 to +0.046 e for PCBM molecule. Only six neighboring atoms of C_{60} experience the strongest influence of the polar side group. For FP, the difference in charges before and after side-chain attachment (from −0.083 to +0.028 e) includes all selected fourteen atoms, which means that the presence of a short charged addend group has bigger impact on the charge redistribution. The side chain length dependence of charge rearrangement for fulleropyrrolidines is shown in Fig. S2.[103]

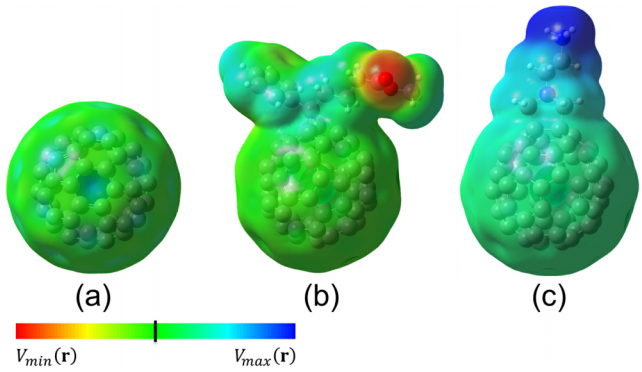

FIG. 3. Molecular electrostatic potential surfaces of fullerene (a), PCBM (b), and naked FP2 cation (c). The electrostatic potentials are plotted on an isoelectronic density surface of 0.004 e a.u.$^{-1}$. The plots show regions ranging from negative (red) via neutral (green) to positive (blue) electrostatic potentials, which are indicated in the scale at the bottom to the plot. The color code of these maps is in the range between −0.019 15 (green) and +0.019 15 a.u. (bluish green) for fullerene, between −0.048 34 (red) and +0.048 34 a.u. (light blue) for PCBM, and between +0.004 (green) and +0.225 a.u. (blue) for FP. It should be pointed out that electrostatics of these systems is computed under ideal conditions (low concentration, $T = 0$ K) and the dynamics and entropic effects are not included into consideration.

It worth noting that QM calculation of MESPs is performed in "ideal" for electrostatics conditions (an infinitely dilute solution, at low temperature/large Bjerrum length and no solvent effects/no screening) for the molecules having optimized geometries. Nevertheless, the shape of their aggregates in aqueous solution can be *a priori* suggested. For example, equally charged side chains will introduce electrostatic repulsion. Therefore, for the fulleropyrrolidines, the more pronounced linear stacking of the molecules in an aggregate is predicted—cylindrical micelles, planar bilayers, etc. For more accurate rationalization of structures, it is necessary to consider thermodynamics, static, and dynamic aspects of solvation.

B. Free energy of solvation

The thermodynamic integration (see Scheme 1[103]) is used to study the free energy of transferring fullerenes from the gas phase into the water phase. The transfer of nanosized

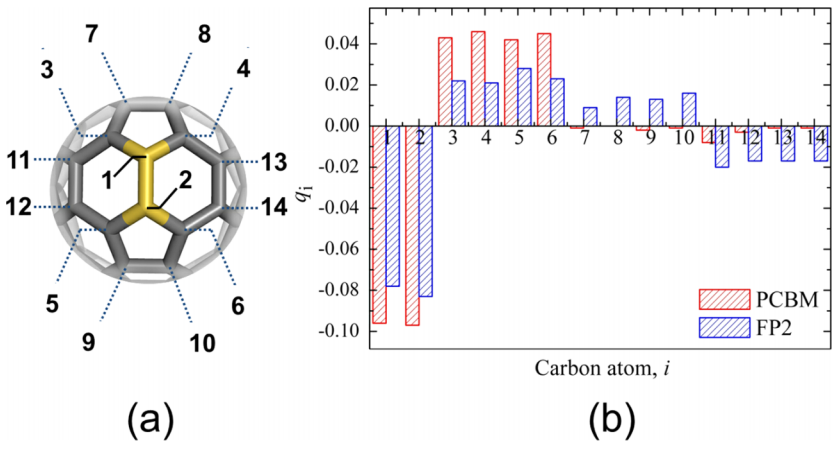

FIG. 4. Variation in Mulliken charges on carbon atoms i of fullerene cage, which are situated in the vicinity of the side chain. (a) Carbons, which side chain is attached to, are shown in yellow. Atoms 3–14 are the nearest neighbors. (b) Computed partial atomic charges for PCBM (red rows) and FP2 (blue rows). The charges on pristine fullerene equal to zero.

carbon-based nanoparticles from gas to aqueous phase is of utmost importance, because similar molecules—air pollutants—can reach the gas-exchange surface in the alveoli, causing various respiratory diseases.[18,19]

The hydration free energy of pristine C_{60} at ambient conditions was calculated recently[35,116–118] by Muthukrishnan *et al.* (−36.10 kJ/mol, 289 K), by Garde *et al.* (−54.1 kJ/mol, 300 K), by Graziano (−18.4 kJ/mol, 298 K), and by Stukalin *et al.* (−2.9 kJ/mol, 298 K). The solvation free energy −17.4 kJ/mol at 298 K is calculated in Refs. 118 and 119 on the basis of experimental C_{60}-solubility in water and sublimation free energy using data by Heymann.[120] We obtain that the solvation energy of C_{60} is −55.27 kJ/mol^{-1} at 298 K. The differences found here can be attributed to the different potentials for water and fullerene used in the simulations. These negative estimates are in line with experimental findings that for the hydration of the aromatic hydrocarbons—toluene and benzene (the latter is considered as one-dimensional analogue of fullerene[100,121])—the free energy of solvation is −3.7 and −3.6 kJ/mol^{-1} at 298 K, respectively.[122] The high negative free energy of hydration (−90.5 mJ/m^2 in terms of surface energy), which is an indicator of the high affinity of fullerenes for water, is found experimentally by Ma *et al.*[123] Recently published results of quantum mechanical density functional theory revealed a negative energy of "C_{60}–H_2O"-cluster formation, i.e., fullerene has attractive interaction with water molecules even though this molecule is hydrophobic.[124]

In the Table S2,[103] we give the results for a transfer of FPs from gas phase into water. Our data have some important lessons (Fig. 5). The most obvious one is that the free energy of solvation for all derivatives is negative, which in the case of purely hydrophobic bare fullerene results in a behaviour quite different than that given by the generally accepted concept of hydrophobicity (in the same manner to potential of mean force for two fullerene spheroids, which reveals a water-mediated repulsion of two hydrophobes from each other). An essential conclusion which can be drawn from this calculation is that the change in free energy of hydration of pristine fullerene is large negative due to the strength of van der Waals interaction between the carbons of spheroid and surrounding water molecules (the key factor is the enormous density of carbon atoms per Å^2, which for fullerene is 0.2).[39,40]

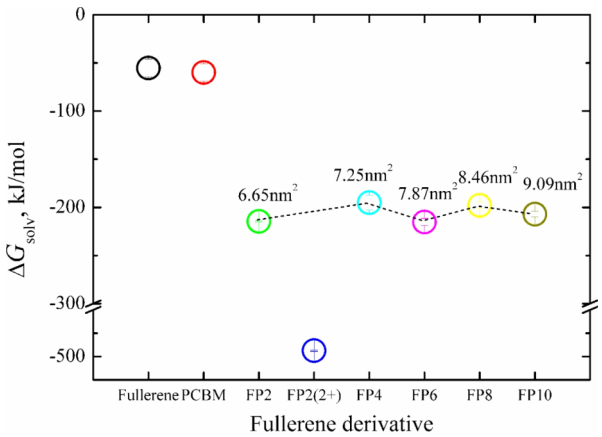

FIG. 5. Free energy of transferring fullerene molecules from gas to water. The dashed line illustrates the difference in solvation energies for homologues series of fulleropyrrolidines. The calculated solvent accessible surface areas in nm^2 are shown as well (the probe radius is 0.14 nm, which corresponds to radius of water). The latter quantity is calculated for the molecules having optimized geometry.

A further observation is that the free energy of hydration is more negative, if the molecule becomes more charged (FP2 cf. FP2, dication) and can itself form more hydrogen bonds with water. Finally, for FP homologues series (Fig. 5, dashed line), we did not observe a clear dependence of ΔG_{solv} on the molecular surface area. One of the possible keys to understanding this fact is "enthalpy-entropy compensation," i.e., the values of ΔG_{solv} are nearly constant through a homologous series, although the changes in the separate enthalpic and entropic terms of the free energy vary substantially and compensate each other.[117,125] Besides, the atomic contributions to the solvation energy might be non-additive and depend on both the neighbor atoms and the molecular geometry, as follows from the analysis by Harris and Pettitt.[126] These assumptions require additional calculations and will be a subject of our next study.

The problem of transfer of C_{60} between two liquid phases—polar and non-polar—is in close relation to (i) the particle translocation across lipid membrane,[8,13–16,18–20,127–131] which often is used as a predictor for the biological activity and (ii) partitioning of fullerenes in different solvents.[45,92,132] To this end, the change in free energy for transferring an isolated C_{60} solute from water to octane is defined as $\Delta\Delta G^t = -64.89$ kJ/mol. Octane is used to imitate the interior of biomembrane;[129] therefore, results for water-alkane free energy of transfer are expected to be in the same range for the transfer from water to the hydrophobic core of lipid membrane, though the latter differs from the isotropic octane phase in chain ordering and packing, density and two-dimensional solute confinement.[133] Our simulation confirms that fullerene partitioning into oily phase (octane) is thermodynamically highly favorable, suggesting its spontaneous diffusion into the membrane. Published measures for the free energy of fullerene transfer from water to octane range between −119.3 and −55.6 kJ/mol,[133–135] showing that our predictions are in agreement with experimental data. This value is very reasonable, as discussed in the context of C_{60} water-to-heptane partitioning by Nielsen *et al.* (−65.27 kJ/mol).[132]

C. Structural analysis: Solvent distribution around nanoparticles

According to aforementioned theories, the hydrophobic effect reflects changes in the structure and thermodynamics of water adjacent to a solute, which depends in turn on the molecular-scale topography of the solute surface. From this perspective, the differences in structure between water in aqueous shells around special site of the solute and water in bulk water may demystify the behaviour of fullerenes in water.

From the radial distribution functions depicted in Fig. 6, it follows that the water molecules are arranged clearly in at least two hydration shells around uncharged C_{60} region of the PCBM and FP2 as well. Similar behaviour is described in previous publications for the pristine fullerene.[36–38,74,82,83,100,136–139] RDF peaks (Fig. 6, black solid

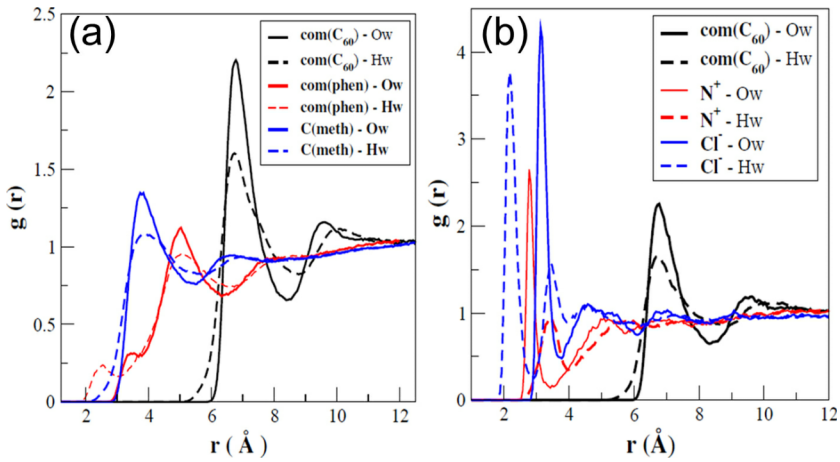

FIG. 6. RDFs between different regions of (a) PCBM, (b) FP2, and oxygen (Ow) and hydrogen (Hw) of water.

and dashed lines) located at $r = 7.83$ Å indicate densely populated solvent molecules[38] in the first solvation shell of the carbon cage of both PCBM and FP2. The peak height corresponding to interfacial layer (water at the fullerene surface) is found to be substantially sharp owing to a high atomistic surface density of fullerene which results in strong van der Waals interactions between solute and solvent molecules. Because of short-range nature of dispersion forces, the rather broad second solvation layer at $r = 9.8$ Å is observed, which means a much less surface-induced structure or bulk-like behaviour of the solvent. The local minimum at 8.5 Å between the first and the second peaks is used to define the number of waters in the first solvation shell of fullerenes. These data for both molecules are collected in Table I.

The fullerene cage of PCBM and FP is surrounded by 60-61 water molecules. This number is comparable to the first solvation shell of pristine fullerene found in other simulations (63 water molecules,[84,140,141] 65,[138] 68,[136] and 70[100]). The small differences can be referred (i) to particular model used, e.g., the combination of LJ parameters of fullerene carbon atoms and water model, which is also echoed in the positions of RDF maxima and minima, and (ii) to the presence of side group attached to PCBM and FP2, which makes inaccessible for water at least two carbon atoms of the spheroid. The same conclusion has been drawn concerning the hydration shells of methylpyrrolidines.[142]

TABLE I. Distance r_{min}, Å corresponding to the first minimum in RDF between selected regions of the solute (see Fig. 6 for more details) and water molecules in the first solvation shell and an average number of solvent molecules in the first solvation shell (n, coordination number, Eq. (2)).

Region of interest	r_{min}, Å	n
PCBM		
C_{60}	8.5	60.23
Phenyl ring	6.4	23.95
Ester moiety	5.4	16.68
FP2		
C_{60}	8.5	60.66
Terminal charged group	3.5	2.81
Chloride ion Cl^-	3.7	6.79

The water structuring around addends is investigated as well. For example, for the case of PCBM phenyl ring, the first RDF shoulder of the hydrogen at 2.5 Å clearly indicates that water "donates" hydrogen bonds to the phenyl group (the corresponding oxygen peak is located at 3.4 Å, as follows from the Fig. 6(a), red dashed and solid lines). This result is in accordance with previous studies on the hydration of benzene.[143,144] Both charged species of FP2 (charged terminal group and chloride counterion, Fig. 6(b), blue and red lines) demonstrate a strong affinity to build hydrogen bonds with water in agreement with QM/MM calculations.[145] The striking first peak of the corresponding Ow-distribution function is centered at 2.8 Å analogously to QM prediction for NH_4^+ and $CH_3NH_3^+$ ions.[76] An average value for the water coordination number of Cl^- is 6.79, which is close to experimental value of 6.[146] More diffuse second and third shells of water around chloride ion are also indicated by the progressively broader bands located near 4.8 and 7 Å.

The orientational profiles of waters are here referred to as the angular distributions as defined in Fig. 2 for the water molecules in the first solvation shell. Near the hydrophobic surface, there is a very broad peak in the distribution (Figs. 7(a) and 8(a) black lines) around $\theta = 90°$ suggesting that water dipoles prefer to be tangential to the PCBM and FP2 spheroid surface. The present distribution resembles those for water near planar graphite/graphene layers and for the pristine fullerene.[41,147,148] The orientation of OH vectors around fullerene cage for both solute surfaces, which is illustrated in the Figs. 7(b) and 8(b), demonstrates two large peaks at $\omega = 0°$ and 105°-108° indicating that one OH bond points away from the solute surface while another OH bond is slightly inclined towards the surface because of water valence HOH angle (~104°). The driving force for the selection of an interfacial structure, called also a dominant one,[149] is (i) the packing forces, which tend to produce a dense molecular layer, and (ii) the tendency of water molecules to maintain a maximal number of hydrogen bonds. The analysis confirms the existence of those dangling–OH bonds for molecules in the first solvation shell, which are observed in previous simulations of graphene hydration (at $\omega = 0°$).[147,150] This phenomenon is considered in details below.

The orientation profile varies dramatically among different parts of the FP2 molecule, clearly classifying some

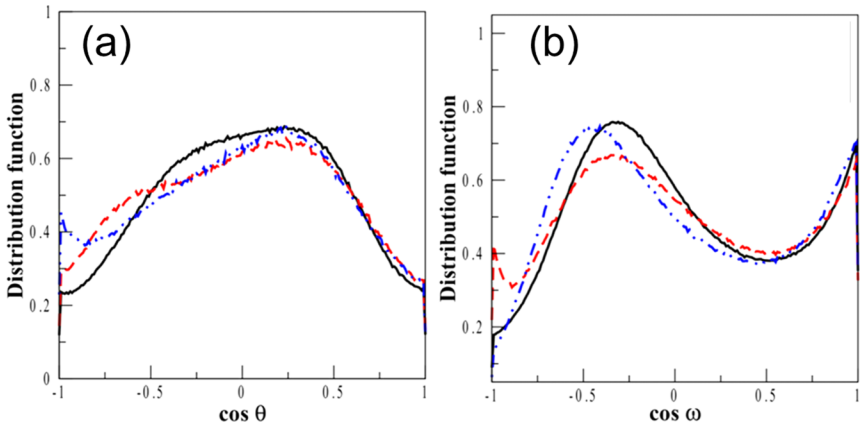

FIG. 7. Ordering of water dipoles near PCBM solute; distributions of $\cos\theta$ (a) and $\cos\omega$ (b) for the solvent in the first solvation shells of carbon spheroid (black solid line), of phenyl group (red dashed line), and of ester moiety (blue dashed-dotted line). The distribution functions are the percentage of the molecules with respect to the total number of molecules in the first solvation shell. The definitions of angles θ and ω are given in the Fig. 2.

anisotropic orientation, which differs markedly from what is observed for carbon cage. The distribution for water dipoles around charged group of FP2 shows a narrow peak at $\cos\theta = 1$ and suggests that the oxygen of water points toward the terminal group forming a very strong hydrogen bond with $-NH_3^+$ (Fig. 8(a)). The same conclusion follows from the Fig. 8(b) for orientation of OH vectors around counterion.

D. Dynamic properties of solvation shells and solute

Apart from the structural aspects, the local dynamics of solvent molecules encompassing a single fullerene derivative can be described by time correlation functions (Eq. (4)). The relaxation of solvent VACF to measure the solvent translational motion in different regions around the solute is shown in Fig. 9. An initial small shoulder observed for all regions of the solute is due to rebound of the water molecule from the shell of their neighbor.[151] It can be seen that VACFs decay approximately to zero within about 0.6 ps. For both solutes, the greater negative dip of VACF in the first solvation shell as compared to bulk water (blue dashed-dotted lines) is observed. Thus, the water molecules in the first solvation shell undergo slower diffusion. The reduced mobility of the solvent molecules, or water retardation, can be attributed to the strong van der Waals interaction between carbonaceous spheroid and solvent.[152,153] The more pronounced effect as result of stronger correlation between charged addend chain of FP2 and water molecules is illustrated in the Fig. 9(b) (red dashed line), which is in agreement with simulations of charged fullerenes in water.[73]

From VACFs, the diffusion constants of water are calculated using Green-Kubo formula (Table II). Experimental diffusion constant for water is 2.299×10^{-9} m^2/s.[154] The values indicate a slowdown in the translational dynamics of water when waters are in vicinity of the solute, because D is considerably less than that of the bulk. The same effect of a hydrophobic surface and ions on water dynamics was obtained in the experiment.[155–159] This change in the water mobility may explain a corresponding change in the physical properties of water in fullerene-containing colloidal solutions.[139] Reorientational rates of water molecules in different regions of solute surfaces are calculated from the molecular dipole moment and OH vector autocorrelation functions (Fig. 10). In the inset, the same plots are shown at initial times. The relaxation times, obtained by fitting KWW function (Eqs. (5) and (6)), are collected in Tables II and III.

All the reorientational correlation functions follow the same general trend that a longer time is required for the relaxation of the orientational correlation of water, which is in close proximity of the solute as compared to the bulk water. This is also clear from the integrated relaxation times included in Tables II and III. The decay is found to be slower for the charged moieties due to stronger interactions of the solvation shell water molecules with the positive terminal group of FP2 or its counterion (>2, a large slowdown factor). Hydrophobic carbon cage is therefore weak water

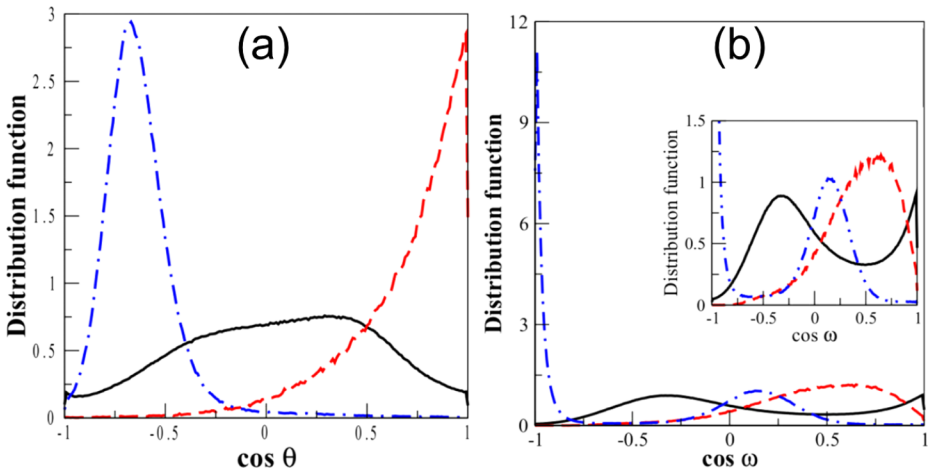

FIG. 8. Ordering of water dipoles near FP2 solute; distributions of $\cos\theta$ (a) and $\cos\omega$ (b) for the solvent in the first solvation shells of carbon spheroid (black solid line), of terminal charged group (red dashed line), and of counterion (blue dashed-dotted line). The distribution functions are the percentage of the molecules with respect to the total number of molecules in the first solvation shell. The definitions of angles θ and ω are given in the Fig. 2.

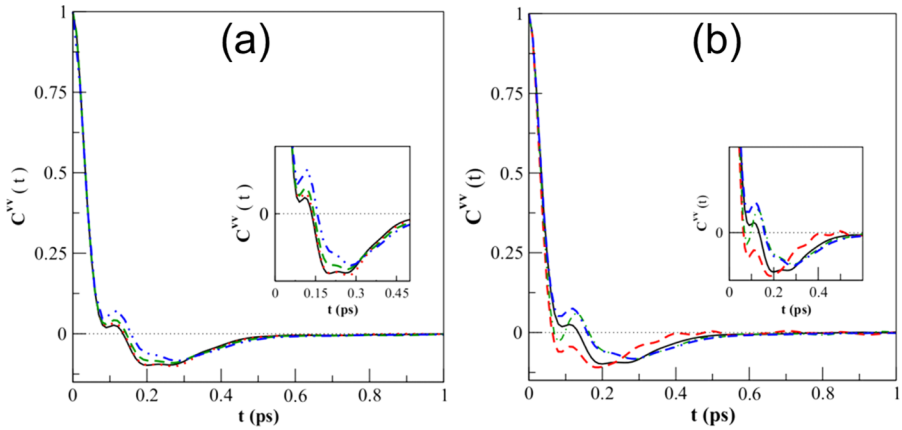

FIG. 9. Normalized velocity autocorrelation functions $C^{vv}(t)$ (Eq. (3)) of water molecules in the first solvation shell of (a) PCBM—water around carbon spheroid (black solid line), phenyl group (red dotted line), ester moiety (green dashed-dotted line), and for bulk water (blue dashed-dotted line) and (b) FP2—around carbon spheroid (black solid line), terminal charged group (red dotted line), counterion (green dashed-dotted line), and for bulk water (blue dashed-dotted line). Magnified views of VACFs at short time have been shown in the insets.

reorientation retardant with respect to hydrophilic or charged groups: the factor always remains below 2, in accordance with structural relaxation of water near hydrophobic surfaces found in experiments[158,160,161] and simulations.[97,106,162]

The reorientational correlation functions show KWW type relaxation. The origin of slowness of water rotation is likely due to the solute surface that dictates the orientation of solvent, restricting relaxation of water. Thus, multiple waters visiting this area near the solute need to accommodate their directions (dipoles, OH–bonds) to the surrounding hydrogen bonds (HB) network; it leads to the correlated motion of solvent molecules. Hotta *et al.*[38] defined this phenomenon as "fluctuating cage" of water near a hydrophobe.

The translational diffusivity of the solutes (Fig. 11) is characterized by the self-diffusion coefficient calculated from the mean square displacement (Eq. (7)). Although we have no experimental results to compare, the predicted value for D_f is in qualitative agreement with other previously simulated results on diffusivity of pristine fullerene in bilayer and bulk water (see Ref. 103). This property exhibits a large sensitivity with respect to the LJ parameters of the carbonaceous spheroid and to the water model used (different parameterizations). Here, we observe that our value is in the range of 10^{-9} m^2/s, which corroborates well the simulation results for the same model used.[128,163] However, it is worth mentioning that even experimental results of diffusion constants of fullerene in organic solvents are rather dissonant.[28]

Despite very similar diffusivities of C_{60}, PCBM, and FPs observed, some preliminary conclusions can be deduced. First of all, even the smallest addend (for example, in PCBM) modelled in this study makes the molecule less mobile, as compared to bare fullerene counterpart, which is related to the enlarged radius of the particle (Stokes' law). Second, the multicharged fulleropyrrolidine (FP2, dication) demonstrates lower translational diffusivity in comparison with FP2. It can be attributed to the larger number of water molecules participating in the formation of strong HBs with two $-NH_3^+$ groups, which effectively enlarge the molecule. A similar result has been obtained by Maciel *et al.*[85] in the process of fullerenol solvation, for which the diffusion constant of hydrophilically modified derivate was found to be significantly decreased owing to the creation of HBs between attached–OH groups and solvent. The impact of molecular size and shape[164] is also clearly seen for the fulleropyrrolidine family: a slowdown in translational diffusion is observed with the lengthening the addend chain.

TABLE II. Diffusion constants D_{water} and reorientational relaxation times of dipole moment vector τ^{μ} of water in the first solvation shell of fullerene derivatives. The average dipolar relaxation times $\langle\tau^{\mu}\rangle$ are calculated by fitting corresponding time correlation function with stretched exponential function (Eqs. (5) and (6)).

		Dipole vector			
Hydration water around	D_{water} (10^{-9} m^2/s)	A	τ^{μ} (ps)	β	$\langle\tau^{\mu}\rangle$ (ps)
PCBM					
C_{60}	1.79	0.9273	7.97	0.855	8.010
Phenyl ring	1.72	0.9560	8.17	0.767	9.136
Ester moiety	1.95	0.9310	7.24	0.861	7.275
Bulk water	2.46	0.9390	5.38	0.853	
FP					
C_{60}	1.87	0.9392	8.280	0.826	8.613
Charged terminal group	1.08	0.9394	16.68	0.740	18.87
Chloride ion Cl^-	1.94	0.9340	8.370	0.883	8.310
Bulk water	2.63	0.9440	5.280	0.841	5.470
Pure water (reference system)	2.55	0.9391	5.344	0.856	5.434

E. Dangling–OH bonds and hydrogen bonds pattern near a solute surface

It was indicated in the previous discussion that dangling –OH bonds, i.e., non-hydrogen bonded groups, may originate from the energetically most favorable way of packing and the tendency of water molecules to build a maximal number of HBs with surroundings near extended hydrophobic surface. The study of water orientation confirms the existence of dangling–OH bonds for all fullerenes in the first solvation shell. The results of a graphical HB analysis of water around FP are illustrated in Fig. 12, which shows a representative simulation snapshot containing several such dangling bonds. It is evident from this snapshot that the number of such structural defects is increased at the bottom hemisphere of fulleropyrrolidine. Around the charged addend chain, all the water hydrogen bonded groups are engaged in the network and in hydrogen bonding with the addend donors and acceptors. Recently,

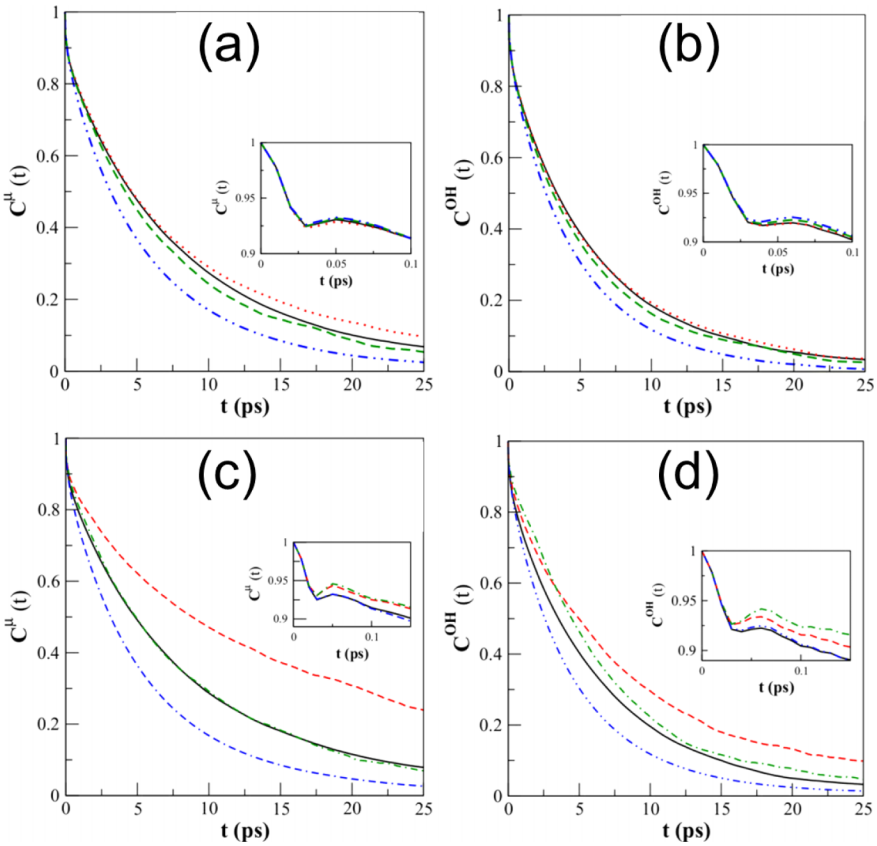

FIG. 10. Reorientational correlation functions of dipole moment vector $C^{\mu}(t)$ (a) and (c) and OH vector $C^{OH}(t)$ (b) and (d) of water molecules in the first solvation shells of PCBM (a) and (b) and FP2 (c) and (d). For the color scheme, see Fig. 9.

the presence of such defects in aqueous solutions containing nonpolar solute has been detected in experiments.[165–168] The authors suggested that translational and rotational retardation of water around a hydrophobe is a consequence of dangling bonds formation, which have slower dynamics.

In the earlier simulations, it was found that the polygon distribution in HB network near hydrophobic surfaces deviates from that in bulk water. For instance, in addition to conventional tetrahedral order, water around an extended hydrophobe forms quasi-planar hexagonal clusters in boat or chair conformations, which are the key elements of ice framework,[91,169–171] so called clathrate structures near hydrophobic solute in solid state. Some phenomenological theories predict the evolution of HB pattern around hydrophobe in liquid water, which is followed by appearance of planar pentagonal cycles.

To analyze these patterns (Fig. 13), the oxygen atoms of waters participating in HB network are connected by lines (Figs. S3-S5[103]), and the several cycles formed are colored in specific tone. This method of visual inspection has been used by Bushuev *et al.*[91] for structural characterization of hydrophobic hydration of rigid spheres of various sizes.

According to our simulations, the topology of the HB network can be described as inhomogeneous and dynamic,

TABLE III. Reorientational relaxation times of OH vector τ^{OH} of water in the first solvation shell of fullerene derivatives. The average dipolar relaxation times $\langle\tau^{OH}\rangle$ are calculated by fitting corresponding time correlation function with stretched exponential function (Eqs. (5) and (6)).

	OH vector			
Hydration water around	A	τ^{OH} (ps)	β	$\langle\tau^{OH}\rangle$ (ps)
PCBM				
C_{60}	0.9235	5.864	0.859	5.85
Phenyl ring	0.9406	5.733	0.813	6.04
Ester moiety	0.9394	5.270	0.833	5.45
Bulk water	0.9283	4.445	0.890	4.37
FP2				
C_{60}	0.9085	6.234	0.900	5.96
Charged terminal group	0.9635	8.156	0.754	9.31
Chloride ion Cl^-	0.9570	6.916	0.943	6.80
Bulk water	0.9370	4.357	0.867	4.39
Pure water	0.9364	4.381	0.871	4.40

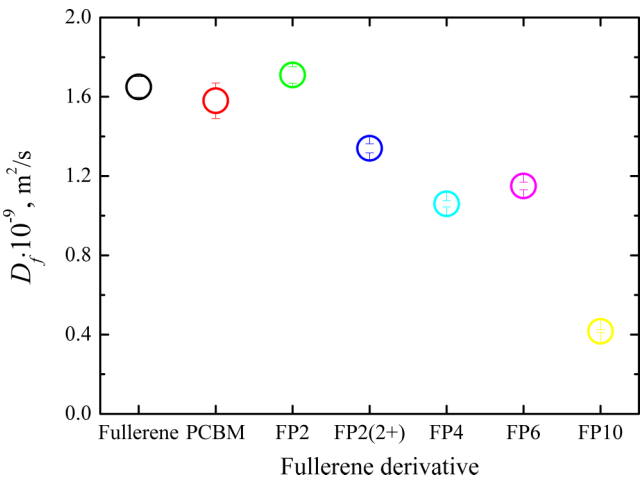

FIG. 11. Coefficients of translational diffusion D_f of pristine fullerene and fullerene derivatives.

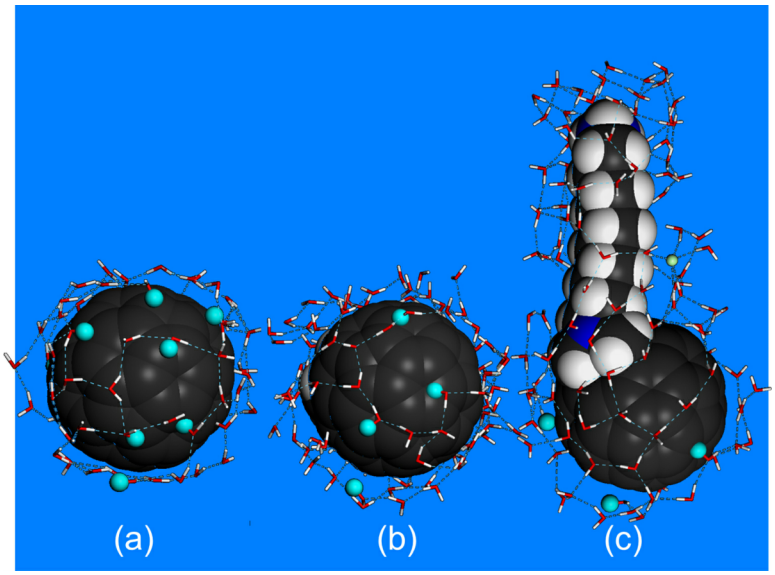

FIG. 12. Dangling–OH groups (free hydrogens of these bonds are shown as cyan beads) in the first solvation shell of fullerene (a) and FP8 molecule: bottom hemisphere (b) and side view (c). Hydrogen bonds are illustrated as dashed lines.

composing of a number of sites with particular spatial distribution and statistics of closed HB cycles. First of all, the most interesting site is the bottom hemisphere of derivatives where the dangling–OH groups are detected. Here, there are large closed cycles (two to three polyhedra) of HB connected water molecules. Most of the structures are opened (i.e., "chains" of HB waters, which are not shown) because of the presence of dangling–OH groups. Here, an aqueous layer close to surface includes regions with reduced density of HB water. These density fluctuations are clearly seen from the Fig. S4,[103] where the HB network is depicted as polyhedra. In fact, one can use a term "dewetting" or "drying" to describe the water structure

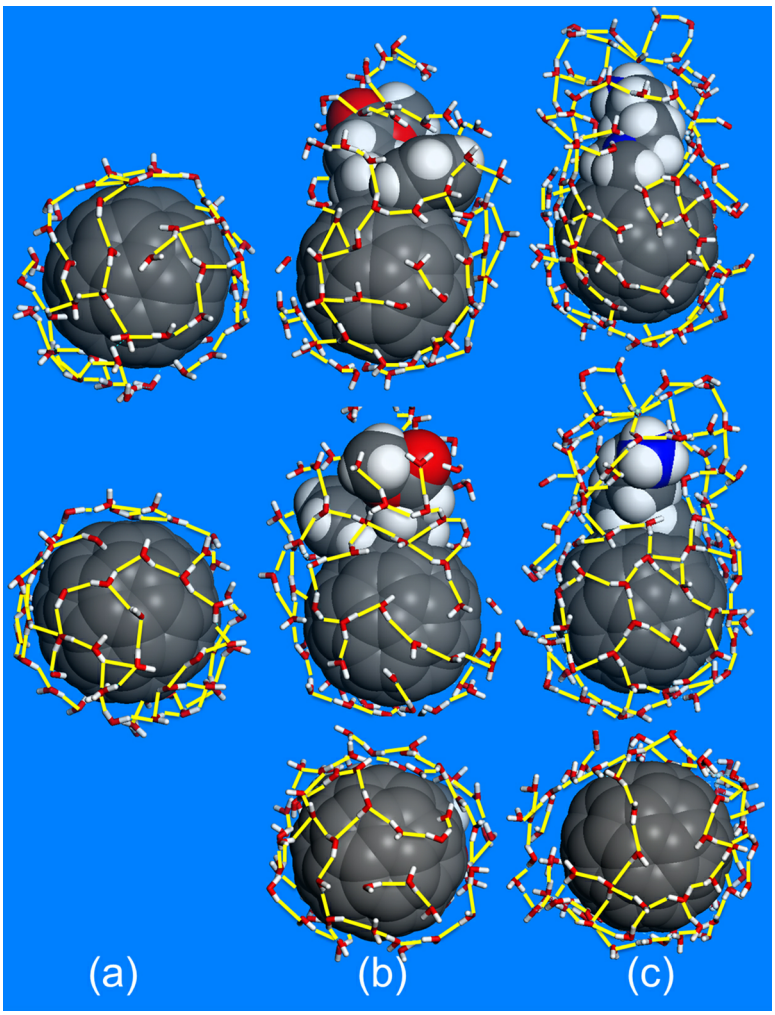

FIG. 13. HB network topology in the first solvation shell of pristine fullerene (column (a)), PCBM (b), and FP (c); here, the hydrogen bonds depict the nearest molecular environment of hydrated particle (yellow lines). The third row shows the bottom hydrophobic caps of PCBM and FP.

at this smooth interfacial region. The same picture is observed for the nearest hydration layer around pristine fullerene. Our results are in qualitative agreement with results by Bushuev *et al.*[91] on the hydration of large van der Waals rigid sphere.

Second, from the equatorial region till the attachment site of the fullerene derivatives, HB network contains a mixture of five- and six-membered cycles (and larger cycles, as indicated in Fig. 13), which is considered in nucleation theory as a prototype of the solid phase with the clathrate-like structure. The same motifs in HB network are obtained from first-principles modeling of water interacting with fullerene.[124] Despite the facts that this structure is non-perfect one (there is no regularity in position of cycles in contrast to predictions by Chaplin[172]) and fluctuates in time, our findings suggest moderately enhanced water structuring in this interfacial region. Here, the surface of a hydrophobe is rather rough than smooth because of the proximity of charged groups. The latter influences the pattern of HB network and acts as suppressor of dangling defects.[173]

Finally, the waters near addends (ester- and phenyl group of PCBM and charged groups of FP family) build the HB network, which is characterized by a combination of four- and five membered cycles, i.e., network reveals greater tetrahedral ordering.

Not only the structural inhomogeneity but also energetic alternation of HBs around fullerene plays a defining role in dictating water-mediated interaction between fullerenes, as follows from the recently published results by Djikaev and Ruckenstein:[174] the phenomenon of oscillatory repulsion is inextricably related to the strength of HBs acting between surface water molecules. It is therefore interesting to examine the averaged values of length between Ow and Hw of vicinal[174] water molecules. As follows from simulations, the longer length of such bonds (Figure S6)[103] as compared to the bulk indicates the weakening of solvent-solvent interaction near the hydrophobe surface (the correlation between hydrogen bond strength and distance is described, e.g., in Ref. 175). In other words, the pattern and energy of HB network of vicinal water differ from its bulk values.

IV. CONCLUDING REMARKS

Fullerene C_{60} spherically symmetric ultrafine particle with diameter ~1 nm has been the subject of intense research, both for its unique chemistry and for the technological significance. Description of hydrated fullerene structures is central to many areas of modern biology and medicine. These nanoparticles have captured the imagination of scientists for their potential application as drug candidates. While some researchers have predicted a bright future for fullerene-based bio-nanotechnology, several studies are raising safety concerns by showing toxic effects of fullerenes, which are correlated with their ability to undergo aggregation in aqueous media of living cell.

The hydrophobic behaviour of fullerenes in water, which at first thought can be described as insolubility and finally precipitation, represents in fact a complex multiscale process. At the molecular level, this insight is even more intriguing, because a bare C_{60} fullerene serves as boundary case between small and large hydrophobic solutes. Because of low solubility in water, the experimental measurements of C_{60} hydrophobic association with nano-resolution are challenging. Therefore, theoretical studies remain the main source of our knowledge about this process on solute size scale.

Simulations reported here describe the properties of water surrounding hydrophobes and the behaviour of both pristine fullerene and several shape amphiphiles in water. Among the objects of the study, fullerene represents a reference system, whereas the investigation of its derivatives allows predicting the effect of various factors influencing the hydration and eventually their self-assembling into clusters. The obtained results can offer relevant and valuable insights into the fundamental properties of water-dispersible fullerene systems.

In this paper, the hydrophobic hydration is considered from two perspectives: water-centric and solute-centric views. Since most of the unique properties of water originate from the pattern of hydrogen bond network and its dynamics, spatial, and orientational aspects of water in solvation shells around the solute surface are analyzed. The static local structure shows that water rearranges around solute surface in a more ordered way than in neat water. Dynamical properties such as translational-rotational mobility, reorientational correlation and occupation time correlation functions of water molecules, and diffusion coefficients are also calculated. Slower dynamics of solvent molecules—water retardation—in the vicinity of the solutes is observed. These waters have restricted motion and cannot organize themselves in tetrahedral manners, as compared to the water in a bulk. Consequently, the "dangling"–OH groups that represent surface defects in water network near a hydrophobic cap of fullerenes are monitored. Large "dry" (free from HB water molecules) regions of C_{60} are observed, which can be considered as a signature of surface dewetting. On the other side, the topological properties of hydrogen bonds pattern reveal the water arrangements with formation of five- and six-membered rings in the nearest environment of the surface, which indicates the improved structuring of water around equatorial region of hydrophobe and near the addend chain. In our opinion, the HB water around fullerene derivatives indeed can be characterized as having inhomogeneous, non-local, and fluctuating structure.

In an effort to provide molecular level insight into the thermodynamics of solute hydration, the free energy of solvation is determined for a family of fullerene particles using thermodynamic integration technique. The change in free energy of hydration is negative for all molecules. Taking into account that the interaction between water atoms and fullerene cage is described purely as dispersion one, the reason for negative solvation free energy lies in strong van der Waals attraction between carbon atoms and solvent. The partitioning of carbon nanoparticles into octane is thermodynamically highly favorable, as compared to water, suggesting the spontaneous diffusion of fullerenes from aqueous phase into oil.

ACKNOWLEDGMENTS

The authors are very grateful to the Center for Information Services and High Performance Computing of the Technische

Universität Dresden for providing CPU time and Dr. Peter Friedel (Leibniz Institute of Polymer Research Dresden) for technical support. O.A.G. wishes to thank Dr. Julia Romanova (University of Surrey) and Marco Werner (Leibniz Institute of Polymer Research Dresden) for useful discussions.

[1]C. M. Lieber and C.-C. Chen, Solid State Phys. **48**, 109 (1994).
[2]R. S. Ruoff, D. S. Tse, R. Malhotra, and D. C. Lorents, J. Phys. Chem. **97**, 3379 (1993).
[3]F. Reisdorfer, O. Haas, P. Le Rendu, and T. P. Nguyen, Synth. Met. **161**, 2544 (2012).
[4]H. Park, R. B. Ambade, and S. H. Lee, J. Nanosci. Nanotechnol. **13**, 7975 (2013).
[5]O. A. Ghazy, "Water-based blend nanoparticles of P3HT and PCBM for the application in organic solar cells," Adv. Polym. Technol. (to be published).
[6]R. Bakry, R. M. Vallant, M. Najam-ul-Haq, M. Rainer, Z. Szabo, C. W. Huck, and G. K. Bonn, Int. J. Nanomed. **2**, 639 (2007).
[7]A. W. Jensen, S. R. Wilson, and D. I. Schuster, Bioorg. Med. Chem. **4**, 767 (1996).
[8]S. Pogodin, M. Werner, J.-U. Sommer, and V. A. Baulin, ACS Nano **6**, 10555 (2012).
[9]N. Todorova, A. J. Makarucha, N. D. M. Hine, A. A. Mostofi, and I. Yarovsky, PLoS Comput. Biol. **9**, e1003360 (2013).
[10]X. Zhao, A. Stirolo, and P. T. Cummings, Biophys. J. **89**, 3856 (2005).
[11]L. Xie, Y. Luo, W. Xi, X. Yang, and G. Wei, Nanoscale **6**, 9752 (2014).
[12]S. Radic, P. Nedumpully-Govindan, R. Chen, E. Salonen, J. M. Brown, P. C. Ke, and F. Ding, Nanoscale **6**, 8340 (2014).
[13]J. Wong-Ekkabut, S. Baoukina, W. Triampo, I. M. Wang, D. P. Tieleman, and L. Monticelli, Nat. Nanotechnol. **3**, 363 (2008).
[14]J. Barnoud, G. Rossi, S. J. Marrink, and L. Monticelli, PLoS Comput. Biol. **10**, e1003873 (2014).
[15]D. Sun, X. Lin, and N. Gu, Soft Matter **10**, 2160 (2014).
[16]M. E. Bozdaganyan, P. S. Orekhov, A. K. Shaytan, and K. V. Shaitan, PLoS ONE **9**, e102487 (2014).
[17]G. B. Skamrova, I. Lapogonov, A. S. Buchelnikov, Y. G. Shckorbatov, S. V. Prylutska, U. Ritter, Y. I. Prylutskyy, and M. P. Evstigneev, Eur. Biophys. J. **43**, 265 (2014).
[18]N. Nisoh, M. Karttunen, L. Monticelli, and J. Wong-Ekkabut, RSC Adv. **5**, 11676 (2015).
[19]J. Barnoud, L. Urbini, and L. Monticelli, J. R. Soc., Interface **12**, 20140931 (2015).
[20]F. Tian, X. Zhang, and W. Dong, Phys. Rev. E **90**, 052701 (2014).
[21]G. V. Andrievsky, V. K. Klochkov, E. L. Karyakina, and N. O. Mchedlov-Petrossyan, Chem. Phys. Lett. **300**, 392 (1999).
[22]L. Bulavin, I. Adamenko, Y. Prylutskyy, S. Durov, A. Graja, A. Bogucki, and P. Scharff, Phys. Chem. Chem. Phys. **2**, 1627 (2000).
[23]D. P. Voronin, A. S. Buchelnikov, V. V. Kostjukov, S. V. Khrapatiy, D. Wyrzykowski, J. Piosik, Y. I. Prylutskyy, U. Ritter, and M. P. Evstigneev, J. Chem. Phys. **140**, 104909 (2014).
[24]P. Kumar, S. Karmakar, and H. B. Bohidar, J. Phys. Chem. C **112**, 15113 (2008).
[25]S. Deguchi, R. G. Alargova, and K. Tsujii, Langmuir **17**, 6013 (2001).
[26]Y. I. Prylutskyy, A. S. Buchelnikov, D. P. Voronin, V. V. Kostjukov, U. Ritter, J. A. Parkinson, and M. P. Evstigneev, Phys. Chem. Chem. Phys. **15**, 9351 (2013).
[27]N. O. Mchedlov-Petrossyan, Chem. Rev. **113**, 5149 (2013).
[28]V. N. Bezmel'nitsyn, A. V. Eletskiĭ, and M. V. Okun', Phys.-Usp. **41**, 1091 (1998).
[29]H. S. Frank and M. W. Evans, J. Chem. Phys. **13**, 507 (1945).
[30]W. Kauzmann, Adv. Protein Chem. **13**, 1 (1959); C. Tanford, Proc. Natl. Acad. Sci. U. S. A. **76**, 4175 (1979).
[31]K. Lum, D. Chandler, and J. D. Weeks, J. Phys. Chem. B **103**, 4570 (1999).
[32]F. H. Stillinger, J. Solution Chem. **2**, 141 (1973).
[33]L. R. Pratt and D. Chandler, J. Chem. Phys. **67**, 3683 (1977).
[34]T. Lazaridis, J. Phys. Chem. B **102**, 3531 (1998).
[35]M. V. Athawale, S. N. Jamadagni, and S. Garde, J. Chem. Phys. **131**, 115102 (2009).
[36]M. Makowski, C. Czaplewski, A. Liwo, and H. A. Scheraga, J. Phys. Chem. B **114**, 993 (2010).
[37]R. C. Remsing and J. D. Weeks, J. Phys. Chem. B **117**, 15479 (2013).
[38]T. Hotta, A. Kimura, and M. Sasai, J. Phys. Chem. B **109**, 18600 (2005).
[39]L. Li, D. Bedrov, and G. D. Smith, Phys. Rev. E **71**, 011502 (2005).
[40]L. Li, D. Bedrov, and G. D. Smith, J. Chem. Phys. **123**, 204504 (2005).
[41]R. Zangi, J. Phys. Chem. B **118**, 12263 (2014).
[42]N. O. Mchedlov-Petrossyan, V. K. Klochkov, and G. V. Andrievsky, J. Chem. Soc., Faraday Trans. **93**, 4343 (1997).
[43]G. V. Andrievsky, V. K. Klochkov, A. B. Bordyuh, and G. I. Dovbeshko, Chem. Phys. Lett. **364**, 8 (2002).
[44]J. Labille, A. Masion, F. Ziarelli, J. Rose, J. Brant, F. Villiéras, M. Pelletier, D. Borschneck, M. R. Wiesner, and J.-Y. Bottero, Langmuir **25**, 11232 (2009).
[45]L. Pospíšil, M. Gál, M. Hromadová, J. Bulíčková, V. Kolivoška, J. Cvačka, K. Nováková, L. Kavan, M. Zukalová, and L. Dunsch, Phys. Chem. Chem. Phys. **12**, 14095 (2010).
[46]A. Tlahuice-Flores and S. Mejía-Rosales, J. Chem. Chem. Eng. **5**, 1034 (2011).
[47]C. Zhang, H. Chen, Y. Chen, Z. Wie, and Z. Pu, Acta Phys.-Chim. Sin. **24**, 1353 (2008).
[48]N. R. Tummala, S. Mehraeen, Y.-T. Fu, C. Risko, and J.-L. Brédas, Adv. Funct. Mater. **23**, 5800 (2013).
[49]J. Idé, D. Fazzi, M. Casalegno, S. V. Meille, and G. Raos, J. Mater. Chem. C **2**, 7313 (2014).
[50]M. Casalegno, S. Zanardi, F. Frigerio, R. Po, C. Carbonera, C. Marra, T. Nicolini, G. Raos, and S. V. Meille, Chem. Commun. **49**, 4525 (2013).
[51]F. Frigerio, M. Casalegno, C. Carbonera, T. Nicolini, S. V. Meille, and G. Raos, J. Mater. Chem. **22**, 5434 (2012).
[52]D. L. Cheung and A. Troisi, J. Phys. Chem. C **114**, 20479 (2010).
[53]J. M. Nápoles-Duarte, M. Reyes-Reyes, J. L. Ricardo-Chavez, R. Garibay-Alonso, and R. López-Sandoval, Phys. Rev. B **78**, 035425 (2008).
[54]A. Kaiser, M. Probst, H. A. Stretz, and F. Hagelberg, Int. J. Mass Spectrom. **365**, 225 (2014).
[55]R. Colle, G. Grosso, A. Ronzani, M. Gazzano, and V. Palermo, Carbon **50**, 1332 (2012).
[56]S. M. Mortuza and S. Banerjee, J. Chem. Phys. **137**, 244308 (2012).
[57]O. A. Guskova, S. R. Varanasi, and J.-U. Sommer, J. Chem. Phys. **141**, 144303 (2014).
[58]H.-Y. Chang, S.-H. Tu, Y.-J. Sheng, and H.-K. Tsao, J. Chem. Phys. **141**, 054906 (2014).
[59]N. Nakashima, T. Ishii, M. Shirakusa, T. Nakanishi, H. Murakami, and T. Sagara, Chem. - Eur. J. **7**, 1766 (2001).
[60]P. Atkins, Pure Appl. Chem. **71**, 927 (1999).
[61]Y. Zhao and G. Chen, in *Fullerenes and Other Carbon-Rich Nanostructures*, edited by J.-F. Nierengarten and D. Bonifazi (Springer, 2014).
[62]P. García-Novo, A. Campo-Cacharrón, E. M. Cabaleiro-Logo, and S. Rodríguez-Otero, Phys. Chem. Chem. Phys. **14**, 104 (2012).
[63]Y.-B. Wang and Z. Lin, J. Am. Chem. Soc. **125**, 6072 (2003).
[64]A. Ikeda, A. Hirata, M. Ishikawa, J.-i. Kikuchi, S. Mieda, and W. Shinoda, Org. Biomol. Chem. **11**, 7843 (2013).
[65]M. J. Frisch, G. W. Trucks, H. B. Schlegel, G. E. Scuseria, M. A. Robb, J. R. Cheeseman, G. Scalmani, V. Barone, B. Mennucci, G. A. Petersson, H. Nakatsuji, M. Caricato, X. Li, H. P. Hratchian, A. F. Izmaylov, J. Bloino, G. Zheng, J. L. Sonnenberg, M. Hada, M. Ehara, K. Toyota, R. Fukuda, J. Hasegawa, M. Ishida, T. Nakajima, Y. Honda, O. Kitao, H. Nakai, T. Vreven, J. A. Montgomery, Jr., J. E. Peralta, F. Ogliaro, M. Bearpark, J. J. Heyd, E. Brothers, K. N. Kudin, V. N. Staroverov, R. Kobayashi, J. Normand, K. Raghavachari, A. Rendell, J. C. Burant, S. S. Iyengar, J. Tomasi, M. Cossi, N. Rega, J. M. Millam, M. Klene, J. E. Knox, J. B. Cross, V. Bakken, C. Adamo, J. Jaramillo, R. Gomperts, R. E. Stratmann, O. Yazyev, A. J. Austin, R. Cammi, C. Pomelli, J. W. Ochterski, R. L. Martin, K. Morokuma, V. G. Zakrzewski, G. A. Voth, P. Salvador, J. J. Dannenberg, S. Dapprich, A. D. Daniels, Ö. Farkas, J. B. Foresman, J. V. Ortiz, J. Cioslowski, and D. J. Fox (Gaussian, Inc., Wallingford, CT, GAUSSIAN 09, Revision A.01 2009).
[66]J. S. Murray and P. Politzer, *Molecular Orbital Calculations for Biological Systems* (Oxford University Press, New York, 1998).
[67]P. Politzer and J. S. Murray, Theor. Chem. Acc. **108**, 134 (2002).
[68]R. Dennington, T. Keith, and J. Millam, GaussView, version 5 (Semichem Inc., Shawnee Mission, KS, 2009).
[69]H. Sun, Macromolecules **28**, 701 (1995).
[70]L. A. Girifalco, J. Phys. Chem. **95**, 5370 (1991).
[71]L.-T. Cheng, J. Dzubiella, J. A. McCammon, and B. Li, J. Chem. Phys. **127**, 084503 (2007).
[72]L. Monticelli, J. Chem. Theory Comput. **8**, 1370 (2012).
[73]M. K. Rana and A. Chandra, J. Chem. Phys. **137**, 134501 (2012).

[74]N. Choudhury, J. Phys. Chem. B **111**, 10474 (2007).
[75]P. N. Govindan, L. Monticelli, and E. Salonen, J. Phys. Chem. B **116**, 10676 (2012).
[76]W. L. Jorgensen and J. Gao, J. Phys. Chem. **90**, 2174 (1986).
[77]M. P. Allen and D. J. Tildesley, *Computer Simulation of Liquids* (Clarendon Press, Oxford, 1987).
[78]D. J. Price and C. L. Brooks III, J. Chem. Phys. **121**, 10096 (2004).
[79]L. M. Ararcón, D. C. Malaspina, E. P. Schultz, M. A. Frechero, and G. A. Appignanesi, Chem. Phys. **388**, 47 (2011).
[80]E. E. Fileti and V. V. Chaban, J. Phys. Chem. Lett. **5**, 1795 (2014).
[81]E. E. Fileti and V. V. Chaban, J. Phys. Chem. B **118**, 7376 (2014).
[82]V. V. Chaban, C. Maciel, and E. E. Fileti, J. Phys. Chem. B **118**, 3378 (2014).
[83]B. P. Lambeth, Jr., C. Junghans, K. Kremer, C. Clementi, and L. Delle Site, J. Phys. Chem. **133**, 221101 (2010).
[84]J. Hernández-Rojas, J. Bretón, J. M. Gomez Llorente, and D. J. Wales, J. Phys. Chem. B **110**, 13357 (2006).
[85]C. Maciel, E. E. Fileti, and R. Rivelino, Chem. Phys. Lett. **507**, 244 (2011).
[86]E. E. Fileti, J. Phys. Chem. B **118**, 12471 (2014).
[87]A. Bartosik, M. Wiśniewska, and M. Makowski, J. Phys. Org. Chem. **28**, 10 (2015).
[88]X. Zhao, J. Phys. Chem. C **112**, 8898 (2008).
[89]S. Mieda, A. Ikeda, Y. Shigeri, and W. Shinoda, J. Phys. Chem. C **118**, 12555 (2014).
[90]R. Rivelino and F. de Brito Mota, Nano Lett. **7**, 1526 (2007).
[91]Yu. G. Bushuev, S. V. Davletbaeva, and V. P. Korolev, Russ. Chem. Bull. **57**, 1811 (2008).
[92]P. S. Redmill, S. L. Capps, P. T. Cummings, and C. McCabe, Carbon **47**, 2865 (2009).
[93]E. M. Kotsalis, R. L. Jaffe, J. H. Walther, T. Werder, and P. Koumoutsakos, in *Annual Research Briefs* (Center for Turbulence Research, 2001), Vol. 283.
[94]L. Martínez, R. Andrade, E. G. Birgin, and J. M. Marítnez, J. Comput. Chem. **30**, 2157 (2009).
[95]H. Kim, D. Bedrov, and G. D. Smith, J. Chem. Theory Comput. **4**, 335 (2008).
[96]L. Li, D. Bedrov, and G. D. Smith, J. Phys. Chem. B **110**, 10509 (2006).
[97]N. Choudhury, J. Phys. Chem. C **111**, 2565 (2007).
[98]J. H. Walther, M. Praprotnik, E. M. Kotsalis, and P. Koumoutsakos, J. Comput. Phys. **231**, 2677 (2012).
[99]S. J. Plimpton, J. Comput. Phys. **117**, 1 (1995).
[100]D. R. Weiss, T. M. Raschke, and M. Levitt, J. Phys. Chem. B **112**, 2981 (2008).
[101]A. Leach, *Molecular Modelling: Principles and Applications* (Prentice Hall, New York, 2001).
[102]H. Sun, J. Phys. Chem. B **102**, 7338 (1998).
[103]See supplementary material at http://dx.doi.org/10.1063/1.4922322 for Figures S1-S7, Tables S1 and S2, and Scheme S1.
[104]T.-X. Xiang and B. D. Anderson, J. Pharm. Sci. **103**, 2759 (2014).
[105]M. Ozmaian and R. Naghdabadi, J. Polym. Sci., Part B: Polym. Phys. **52**, 907 (2014).
[106]Z. Cao, Y. Peng, S. Li, L. Liu, and T. Yan, J. Phys. Chem. C **113**, 3096 (2009).
[107]G. G. Vogiatzis and D. N. Theodorou, Macromolecules **47**, 387 (2014).
[108]F. Kohlrausch, Poggendorff's Ann. Phys. **195**, 337 (1863).
[109]G. Williams and D. C. Watts, Trans. Faraday Soc. **66**, 80 (1970).
[110]J. P. Boon and S. Yip, *Molecular Hydrodynamics* (Dover Publications, New York, 1980).
[111]A. Luzar and D. Chandler, Nature **379**, 55 (1996).
[112]W. Humphrey, A. Dalke, and K. Schulten, J. Mol. Graphics **14**, 33 (1996).
[113]The PyMOL Molecular Graphics System, version 1.2r3pre, Schrödinger, LLC, 2008.
[114]DS Visualizer®, v. 4.0, Accelrys Software Inc., 2013.
[115]X. Zhang, X.-D. Li, L.-X. Ma, and B. Zhang, RSC Adv. **4**, 60342 (2014).
[116]A. Muthukrishnan and M. V. Sangaranarayanan, Chem. Phys. **331**, 200 (2007).
[117]G. Graziano, Chem. Phys. Lett. **499**, 79 (2010).
[118]E. B. Stukalin, M. V. Korobov, and N. V. Avramenko, J. Phys. Chem. B **107**, 9692 (2003).
[119]Y. Marcus, A. L. Smith, M. V. Korobov, A. L. Mirakyan, N. V. Avramenko, and E. B. Stukalin, J. Phys. Chem. B **105**, 2499 (2001).
[120]D. Heymann, Carbon **34**, 627 (1996).
[121]J.-C. Huang, Fluid Phase Equilib. **237**, 186 (2005).
[122]G. Graziano and B. Li, J. Phys. Chem. B **105**, 10367 (2001).
[123]X. Ma, B. Wigington, and D. Bouchard, Langmuir **26**, 11886 (2010).
[124]J. I. Choi, S. Snow, J.-H. Kim, and S. S. Jang, Environ. Sci. Technol. **49**, 1529 (2015).
[125]P. Widom, P. Bhimalapuram, and K. Koga, Phys. Chem. Chem. Phys. **5**, 3085 (2003).
[126]R. C. Harris and B. M. Pettitt, Proc. Natl. Acad. Sci. U. S. A. **111**, 14681 (2014).
[127]M. Bortolus, C. Parisio, A. L. Maniero, and A. Ferrarini, Langmuir **27**, 12560 (2011).
[128]D. Bedrov, G. D. Smith, H. Davande, and L. Li, J. Phys. Chem. B **112**, 2078 (2008).
[129]J. Barnoud, G. Rossi, and L. Monticelli, Phys. Rev. Lett. **112**, 068102 (2014).
[130]X. C. He, M. Lin, F. Li, B. Y. Sha, F. Xu, Z. G. Qu, and L. Wang, Nanomedicine **10**, 121 (2015).
[131]C.-c. Chiu, W. Shinoda, R. H. DeVane, and S. O. Nielsen, Soft Matter **8**, 9610 (2012).
[132]C.-c. Chiu, R. DeVane, M. L. Klein, W. Shinoda, P. B. Moore, and S. O. Nielsen, J. Phys. Chem. B **114**, 6394 (2010).
[133]G. Rossi, J. Barnoud, and L. Monticelli, Phys. Scr. **87**, 058503 (2013).
[134]D. Heymann, Fullerene Sci. Technol. **4**, 509 (1996).
[135]T. Yoshihara, M. Murai, Y. Tamaki, A. Furube, and R. Katoh, Chem. Phys. Lett. **394**, 161 (2004).
[136]G. Colherinhas, T. L. Fonseca, and E. E. Fileti, Carbon **49**, 187 (2011).
[137]J. A. Morrone, J. Li, and B. J. Berne, J. Phys. Chem. B **116**, 378 (2012).
[138]R. Rivelino, A. M. Maniero, F. V. Prudente, and L. S. Costa, Carbon **44**, 2925 (2006).
[139]K.-C. Fang and C.-I. Weng, J. Colloid Interface Sci. **318**, 188 (2008).
[140]R. Ludwig and A. Appelhagen, Angew. Chem., Int. Ed. **44**, 811 (2005).
[141]*Solvation Effects on Molecules and Biomolecules, Computational Methods and Applications*, edited by S. Canuto (Springer Science, 2008).
[142]S. D. Snow, K. C. Kim, K. J. Moor, S. S. Jang, and J.-H. Kim, Environ. Sci. Technol. **49**, 2147 (2015).
[143]P. Schravendijk and N. F. A. van der Vegt, J. Chem. Theory Comput. **1**, 643 (2005).
[144]N. Galamba, J. Phys. Chem. B **117**, 2153 (2013).
[145]S. Pezeshki and H. Lin, J. Comput. Chem. **35**, 1778 (2014).
[146]P.-A. Bergström, J. Lindgren, and O. Kristiansson, J. Phys. Chem. **95**, 8575 (1991).
[147]M. C. Gordillo and J. Martí, Phys. Rev. B **78**, 075432 (2008).
[148]N. Choudhury, J. Chem. Phys. **125**, 034502 (2006).
[149]C.-Y. Lee, J. A. McCammon, and P. J. Rossky, J. Chem. Phys. **80**, 4448 (1984).
[150]G. Cicero, J. K. Grossman, E. Schwegler, F. Gygi, and G. Galli, J. Am. Chem. Soc. **130**, 1871 (2008).
[151]D. A. Zichi and P. J. Rossky, J. Chem. Phys. **84**, 2814 (1986).
[152]C. J. Wang, C. C. Hua, and S. A. Chen, J. Phys. Chem. B **118**, 9964 (2014).
[153]N. Galamba, J. Phys. Chem. B **118**, 4169 (2014).
[154]M. Holz, S. R. Heil, and A. Sacco, Phys. Chem. Chem. Phys. **2**, 4740 (2000).
[155]A. A. Bakulin, C. Liang, T. la Cour Jansen, D. A. Wiersma, H. J. Bakker, and M. S. Pshenichnikov, Acc. Chem. Res. **42**, 1229 (2009).
[156]A. A. Bakulin, M. S. Pshenichnikov, H. J. Bakker, and C. Petersen, J. Phys. Chem. A **115**, 1821 (2011).
[157]J. Qvist and B. Halle, J. Am. Chem. Soc. **130**, 10345 (2008).
[158]S. Wi, J. Spano, and W. A. Ducker, J. Phys. Chem. C **114**, 14986 (2010).
[159]S. T. van der Post, K.-J. Tielrooij, J. Hunger, E. H. G. Backus, and H. J. Bakker, Faraday Discuss. **160**, 171 (2013).
[160]A. Politano and G. Chiarello, J. Chem. Phys. **139**, 064704 (2013).
[161]J. T. Titantah and M. Karttunen, J. Am. Chem. Soc. **134**, 9362 (2012).
[162]M. K. Rana and A. Chandra, J. Chem. Phys. **138**, 204702 (2013).
[163]A. Jusufi, R. H. DaVane, W. Shinoda, and M. L. Klein, Soft Matter **7**, 1139 (2011).
[164]R. Haselmeier, M. Holz, M. M. Kappes, R. H. Michel, and D. Fuchs, Ber. Bunsengesellschaft Phys. Chem. **98**, 878 (1994).
[165]J. G. Davis, B. M. Rankin, K. P. Gierszal, and D. Ben-Amotz, Nat. Chem. **5**, 796 (2013).
[166]P. N. Perera, K. R. Fega, L. Lawrence, E. J. Sundstrom, J. Tomlinson-Phillips, and D. Ben-Amotz, Proc. Natl. Acad. Sci. U. S. A. **106**, 12230 (2009).
[167]J. Tomlinson-Phillips, J. G. Davis, D. Ben-Amotz, D. Spångberg, L. Pejov, and K. Hermansson, J. Phys. Chem. A **115**, 6177 (2011).
[168]J. G. Davis, K. P. Gierszal, P. Wang, and D. Ben-Amotz, Nature **491**, 582 (2012).
[169]T. Head-Gordon, Proc. Natl. Acad. Sci. U. S. A. **92**, 8308 (1995).
[170]E. K. Peter, M. Agarwal, B. Kim, I. V. Pivkin, and J.-E. Shea, J. Chem. Phys. **141**, 22D511 (2014).

[171]D. Lee, E. Schwegler, and Y. Kanai, J. Phys. Chem. C **118**, 8508 (2014).
[172]M. F. Chaplin, "Water structuring at colloidal surfaces," in *Surface Chemistry in Biomedical and Environmental Science*, NATO Security through Science Series edited by J. Blitz and V. Gun'ko (Springer, Dordrecht, The Netherlands, 2006), Vol. 228, p. 1.
[173]J. G. Davis, S. R. Zukowski, B. M. Rankin, and D. Ben-Amotz, "Influence of a neighboring charged group on hydrophobic hydration shell structure," J. Phys. Chem. B (unpublished).
[174]Y. S. Djikaev and E. Ruckenstein, J. Phys. Chem. Lett. **6**, 1761 (2015).
[175]M. Huš and T. Urbic, J. Chem. Phys. **136**, 144305 (2012).